Research Letter **DOI:** 10.15541/jim20240279

Mechanism for Hydrothermal-carbothermal Synthesis of AlN Nanopowders

FENG Guanzheng[1,2,3], YANG Jian[1,2], ZHOU Du[1,2], CHEN Qiming[1,2,3], XU Wentao[1,2], ZHOU Youfu[1,2]

(1. Key Laboratory of Optoelectronic Materials Chemistry and Physics, Fujian Institute of Research on the Structure of Matter, Chinese Academy of Sciences, Fuzhou 350002, China; 2. Fujian Science & Technology Innovation Laboratory for Optoelectronic Information of China, Fuzhou 350108, China; 3. University of Chinese Academy of Sciences, Beijing 100039, China)

Abstract: Currently, the carbothermal reduction-nitridation (CRN) process is the predominant method for preparing aluminum nitride (AlN) powder. Although AlN powder prepared by CRN process exhibits high purity and excellent sintering activity, it also presents challenges such as the necessity for high reaction temperatures and difficulties in achieving uniform mixing of its raw materials. This study presents a comprehensive investigation into preparation process of AlN nanopowders using a combination of hydrothermal synthesis and CRN. In the hydrothermal reaction, a homogeneous composite precursor consisting of carbon and boehmite (γ-AlOOH) is synthesized at 200 ℃ using aluminum nitrate as the aluminum source, sucrose as the carbon source, and urea as the precipitant. During the hydrothermal process, the precursor develops a core-shell structure, with boehmite tightly coated with carbon (γ-AlOOH@C) due to electrostatic attraction. Compared with conventional precursor, the hydrothermal hybrid offers many advantages, such as ultrafine particles, uniform particle size distribution, good dispersion, high reactivity, and environmental friendliness. The carbon shell enhances thermodynamic stability of γ-Al_2O_3 compared to the corundum phase (α-Al_2O_3) by preventing the loss of the surface area in alumina. This stability enables γ-Al_2O_3 to maintain high reactivity during CRN process, which initiates at 1300 ℃, and concludes at 1400 ℃. The underlying mechanisms are substantiated through experiments and thermodynamic calculations. This research provides a robust theoretical and experimental foundation for the hydrothermal combined carbothermal preparation of non-oxide ceramic nanopowders.

Key words: aluminum nitride; carbothermal reduction-nitridation; mechanism; hydrothermal synthesis; precursor

Recently, aluminum nitride (AlN) has garnered significant attention due to its exceptional properties, including high intrinsic thermal conductivity (320 W/(m·K)), superior insulation performance (>10^{14} Ω·m), low dielectric constant and loss, a thermal expansion coefficient (4.2×10^{-6} K^{-1}) close to that of semiconductor silicon, and non-toxicity[1-4]. The aforementioned characteristics render AlN a highly promising substrate and packaging material for electronic applications[5-6]. However, the sintering of AlN ceramics is challenging due to their robust covalent bonds and low diffusion coefficient[7]. The use of ultrafine powders provides a feasible solution to alleviate the sintering difficulty associated with AlN ceramics. AlN can be prepared using a variety of techniques, such as the carbothermal reduction-nitridation (CRN) method[8-9], direct nitridation[10-11], self-propagating high-temperature synthesis[12], and gas reduction-nitridation method[13-16]. The direct nitridation and CRN have been widely used in industry. However, the purity of AlN prepared by direct nitridation remains low, and the particles agglomerate seriously, necessitating an inevitable follow-up grinding process. AlN powders with excellent stability, easy sinterability, and high purity can be prepared using the traditional CRN process. Nevertheless, this method also encounters several limitations, including challenges in

Received date: 2024-06-07; **Revised date:** 2024-09-02; **Published online:** 2024-09-02
Foundation item: National Key Research and Development Program of China (2022YFB3708500, 2023YFB3611000); Fujian Science & Technology Innovation Laboratory for Optoelectronic Information of China (2020ZZ109)
Biography: FENG Guanzheng (1998–), male, Master candidate. E-mail: fengguanzheng01@163.com
冯关正(1998–), 男, 硕士研究生. E-mail: fengguanzheng01@163.com
Corresponding author: ZHOU Youfu, professor. E-mail: yfzhou@fjirsm.ac.cn
周有福, 研究员. E-mail: yfzhou@fjirsm.ac.cn

uniformly mixing the raw materials, the necessity for a high calcination temperature (>1600 ℃), and an extended reaction time required to achieve complete nitridation. Therefore, it is difficult to obtain high-quality AlN nanopowders by traditional CRN method. Obviously, highly reactive raw materials and homogeneously mixed precursors (Al_2O_3+C) are critical prerequisites for the production of high-quality ultrafine AlN powders.

The hydrothermal synthesis is a convenient method for preparing inorganic particles[17], and has also been employed for synthesizing nanocarbon materials[18-20]. In addition to being environmentally friendly, hydrothermal synthesis yields powders with a homogeneous, nanoscale particle size distribution, good dispersion, high reactivity, and no contaminants typically associated with physical pulverization. Furthermore, the morphology of the particles can be precisely controlled by adjusting the reaction conditions. We prepared a precursor composed of boehmite (pyrolysis to γ-Al_2O_3) and carbon using hydrothermal synthesis[21-23]. The CRN technique was then applied to these precursors to produce AlN and AlON nanopowders with high sintering activity. Transparent AlN ceramics with a thermal conductivity of 191.8 W/(m·K) were successfully fabricated by hot-pressing sintering at 1800 ℃ for 3 h using the nanopowders with 3% (in mass) CaF_2 as an additive[22]. Transparent AlON ceramics with a line transmittance of more than 80% were prepared by pressureless sintering at 1880 ℃ using AlON powders obtained *via* the hydrothermal-carbothermal method[23].

Our previous research primarily concentrated on the impact of various experimental parameters on the synthesis of ultrafine powders. In this study, we investigated the mechanism underlying both hydrothermal and CRN processes while also explaining why hydrothermal precursors confer advantages in CRN reactions.

1 Experimental

1.1 Materials and methods

Aluminum nitrate ($Al(NO_3)_3·9H_2O$, aluminum source), urea ($CO(NH_2)_2$, precipitant), and sucrose ($C_{12}H_{22}O_{11}$, carbon source) are analytical pure reagents, which were purchased from Shanghai Titan Technology Co., Ltd., Shanghai, China. The starting materials mentioned above were dissolved in 100 mL deionized water. The content of aluminum nitrate in aqueous solution was 0.05 mol, while the molar ratio of urea to aluminum nitrate was fixed at 2 (U/Al=2) and the molar ratio of carbon (12 times the amount of sucrose) to aluminum nitrate was fixed at 4. Subsequently, this solution was transferred into a Teflon lined stainless steel autoclave with a capacity of 200 mL and heated to 200 ℃ for 12 h. After cooling, the product was filtered and washed three times with deionized water. The precipitate was processed with vacuum freeze drying to obtain precursors (γ-AlOOH@C). The precursors were then subjected to CRN in a graphite furnace at a heating rate of 10 ℃/min until reaching the target temperature of 1100–1600 ℃, which was then held for 4 h under nitrogen flow at a rate of 1 L/min. Finally, the residual carbon in nitridation products was removed through calcination at 700 ℃ in air for 30 min.

1.2 Characterization

The nitridation products were investigated for phase composition by an X-ray diffractometer (XRD, Rigaku Miniflex600, Tokyo, Japan) using CuKα radiation operated at 40 kV and 15 mA. The morphology and particle size of the precursor and AlN nanopowder were observed using a field emission scanning electron microscope (FESEM, Hitachi SU8010, Tokyo, Japan). The precursor was characterized for its microstructure and elemental composition using a transmission electron microscope (TEM, FEI Tecnai G^2F20, Hillsboro, OR, USA). The high-angle annular dark field (HAADF) and mapping images were performed on the Tecnai G^2F20 in scanning mode. The functional groups of hydrothermal carbon and precursors were analyzed using a Fourier transform infrared spectroscope (FTIR, Bruker Optics, Karlsruhe, Germany) with a spectral resolution of 4.0 cm^{-1}. The specific surface area and porosity of γ-Al_2O_3, obtained by removing carbon after calcining the precursor at 1200 ℃, were determined using an automatic surface area and porosity analyzer (Micromeritics ASAP2020C+M, Norcross, USA). The elemental and chemical states of the precursors were qualitatively and quantitatively analyzed by an X-ray photoelectron energy dispersive spectrometer (XPS, Thermo Scientific ESCALAB 250Xi, Waltham, USA).

2 Results and discussion

2.1 Core-shell structure of the precursor

XRD pattern and corresponding FESEM image of the precursor synthesized by hydrothermal process are displayed in Fig. S1. XRD pattern of the precursor exhibits strong correlation with the reference boehmite (γ-AlOOH, JCPDS NO.76-1871), indicating the presence of both amorphous carbon and crystalline boehmite, without impurity phase detected. The morphology and size of the precursor were observed, revealing a star fruit shape, with dimensions ranging from 600 to 800 nm.

As depicted in Fig. 1(a), the precursor features a core-shell

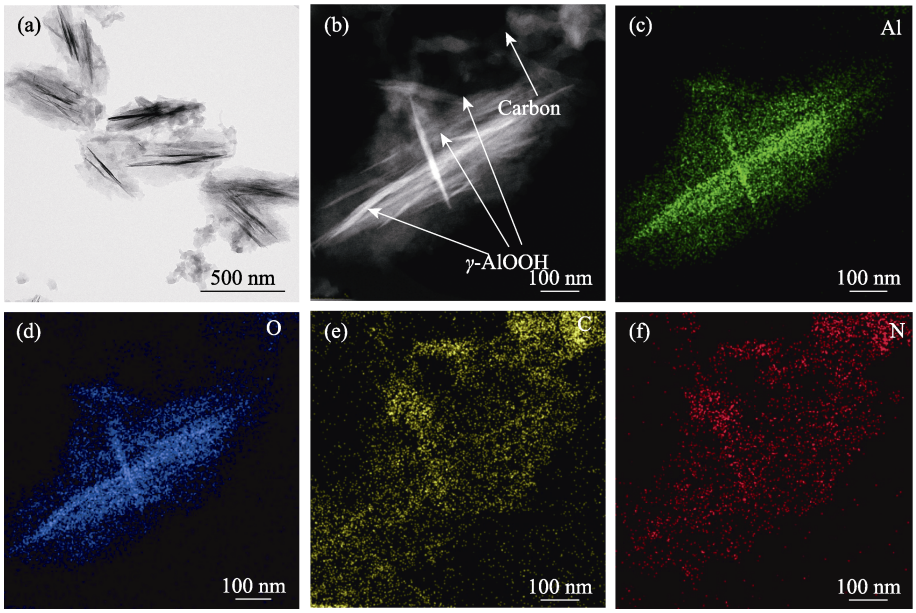

Fig. 1 TEM image, HAADF image and elemental mappings of the precursor
(a) TEM; (b) HAADF; (c-f) Elemental mappings of (c) Al, (d) O, (e) C, and (f) N

structure. The boehmite displays a well-defined shape composed of multiple stacked thin strips, which appear as black bands in the TEM bright-field image. The thickness of the boehmite crystallite is about 20 nm (Fig. S2). In contrast, the carbon exists in an amorphous state, resembling gray cloud wrapped around the surface of the boehmite.

The core-shell structure of carbon-coated boehmite is further validated by HAADF image. As illustrated in Fig. 1(b), the boehmite region appears brighter due to the higher atomic number of aluminum, whereas the hydrothermal carbon exhibits foggy appearance due to the smaller atomic numbers of its constituent elements. Elemental mappings (Fig. 1(c-e)) indicate that aluminum and oxygen are primarily distributed within the needle-like structure of boehmite, while carbon predominantly comprises the amorphous coating. Furthermore, the presence of nitrogen doping in the hydrothermal carbon is evident in Fig. 1(f), consistent with XPS analyses (Fig. S3).

In the structure of boehmite, each Al^{3+} ion is coordinated by two bridging hydroxyl and four oxygen ions[24], where the electrical properties of the surface can be tailored by adjusting pH of the solution (Fig. 2(a)). According to the results of XPS (Fig. S3) and FTIR (Fig. S4) spectra, the carbon structure consists of C=C and C−C bonds, forming a

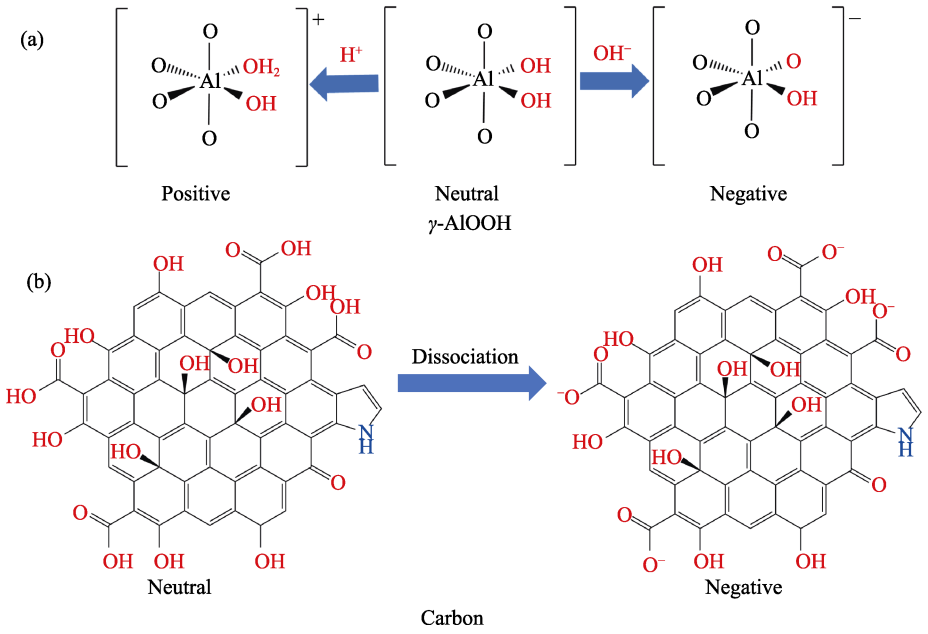

Fig. 2 (a) γ-AlOOH and (b) carbon electrically charged in an aqueous solution

skeleton interlinked with numerous oxygen-containing functional groups such as −OH, −COOH, and a minor amount of −NH (Fig. 2(b)). In weak alkaline systems (pH 8.5), carboxylic acids are fully ionized, resulting in a negatively charged surface on the carbons.

Zeta potentials were subsequently measured at different pH values for dispersions of hydrothermal carbon and boehmite (Fig. 3(a)). Within the acidic to alkaline range, the Zeta potential of the hydrothermal carbons remains negative, fluctuating around −20 mV, indicating that the acidic groups attached to the carbon surface impart negative charge to the hydrothermal carbon. The result is consistent with the behavior of graphene oxide, which possesses a similar structure[25-26]. Conversely, the Zeta potential of the dispersion solution of boehmite remains positive (16.48–33.60 mV) when pH is below 10. It reaches the isoelectric point and becomes negative at pH 11. Therefore, co-precipitation can be achieved over a wide pH range of 3 to 10 as positively charged boehmite and negatively charged carbon interact electrostatically to form a neutral homogeneous precursor (γ-AlOOH@C). As previously discussed, positively charged boehmite crystallites are preferentially formed in an aqueous solution, attracting negatively charged carbon through electrostatic action. During the hydrothermal processes, carbon particles adsorb onto the surface of boehmite and aggregate, facilitating the continuous growth of the carbon shell (Fig. 3(b)). This provides evidence that the hydrothermal carbon generated in the latter stage can form a uniform precursor with the boehmite generated in the earlier stage. After CRN, the precursor yields pure AlN (Fig. S5–Fig. S7).

2.2 Phase transformation

Fig. 4(a) displays typical XRD patterns of the samples obtained after CRN at temperatures ranging from 1100 to 1600 ℃. The products synthesized at 1100 and 1200 ℃ are identified as γ-Al_2O_3, resulting from the pyrolysis of boehmite. As the temperature increases, the nitridation occurs at 1300 ℃ and is completed at 1400 ℃. According to the TGA curve (Fig. S8), the calcined product exhibits a carbon mass fraction of 10.36%. Fig. S9 shows that the resulting AlN nanopowder exhibits a spherical morphology following carbon removal at 700 ℃.

Fig. 4(b) displays XRD patterns of the nitridation products of precursors (Al : U : C=1 : 2 : (0, 1, 2, 3, 4)) at 1500 ℃. For the precursor (C/Al=0) without carbon, the resulting product phase is α-Al_2O_3. As the sucrose

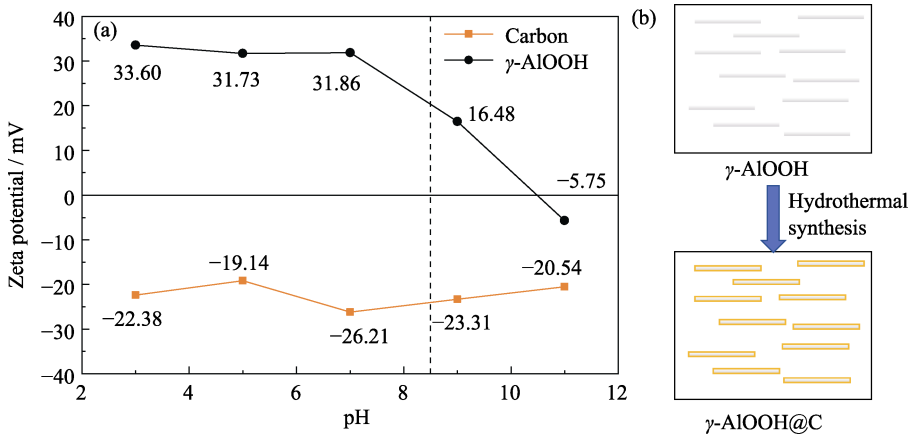

Fig. 3　(a) Zeta potential of γ-AlOOH and carbon dispersions at different pH and (b) mechanism of precursor formation

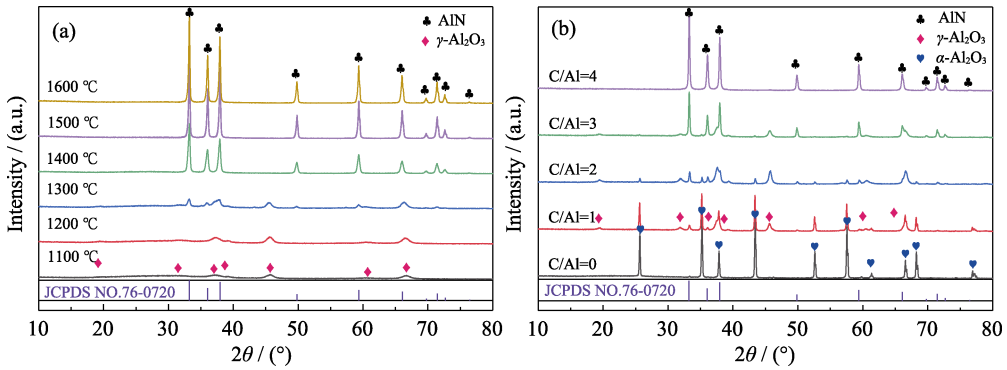

Fig. 4　XRD patterns of the nitridation products synthesized at (a) different temperatures and (b) different C/Al molar ratios at 1500 ℃

content increases, the diffraction peak intensity of α/γ-Al_2O_3 decreases with the intensity of AlN peaks increasing. For precursors with C/Al=4, complete nitridation is achieved, resulting in the formation of pure-phase AlN.

Notably, only the diffraction peaks of γ-Al_2O_3 are observed except for AlN, indicating that the phase transition of alumina from gamma to alpha is effectively suppressed. The finding agrees with literature[27-29], likely due to the high specific surface of ultrafine alumina particles, which allows γ-Al_2O_3 to be directly nitrided without transitioning through α-Al_2O_3 intermediates. A detailed thermodynamic analysis will be presented in subsequent discussion.

2.3 Thermodynamic mechanism

α-Al_2O_3 is widely acknowledged as the thermodynamically stable phase of alumina, with other phases of alumina converting to it at elevated temperatures[30-31]. Boehmite converts to γ-Al_2O_3 at 550 ℃ and subsequently transforms into α-Al_2O_3 when heated above 1200 ℃[30]. However, in this work, alumina remained in γ-Al_2O_3 phase throughout the CRN process, even when subjected to temperatures that exceed the phase transition temperature.

Here, the high-temperature stability of γ-Al_2O_3 and α-Al_2O_3 is quantitatively explained based on their different surface energies through thermodynamic calculations. The enthalpy difference between γ-Al_2O_3 and α-Al_2O_3 at room temperature, assuming zero surface area, is 13.4 kJ/mol[32], and the entropy change associated with the transition from α-Al_2O_3 to γ-Al_2O_3 is 5.7 J/(K·mol)[33]. This suggests that as the temperature increases, the Gibbs free energy for the transformation of α-Al_2O_3 to γ-Al_2O_3 decreases. Table 1 summarizes the surface thermodynamic properties of γ-Al_2O_3 and α-Al_2O_3, showing that the surface energy of α-Al_2O_3 is greater than that of γ-Al_2O_3. This suggests that when the specific surface area is sufficiently large, the Gibbs free energy of α-Al_2O_3 becomes higher than that of γ-Al_2O_3, resulting in the stabilization of γ-Al_2O_3 as the thermodynamically stable phase.

Table 1 Compilation of measured and calculated surface energies in literature

Phase	Surface energy/ ($J·m^{-2}$)	Ref.	Method
α-Al_2O_3	2.04	[34]	MD simulation
	2.64	[33]	High-temperature calorimetry
	2.57	[35]	Static lattice calculation
	2.03	[36]	MD simulation
	4.89	[37]	*Ab initio* calculation
γ-Al_2O_3	0.79	[34]	MD simulation
	1.66	[33]	High-temperature calorimetry
	1.53	[38]	High-temperature calorimetry

The relationship between Gibbs free energy and surface area can be calculated using equation (1).

$$\Delta_r G=\Delta_r H-T\Delta_r S+A\Delta\gamma \quad (1)$$

Where $\Delta_r G$ is the Gibbs free energy change of the reaction, J; $\Delta_r H$ is the enthalpy change of the reaction, J; $\Delta_r S$ is the entropy change of the reaction, $J·K^{-1}$; T is the thermodynamic temperature, K; A is the surface area, m^2; $\Delta\gamma$ is the surface energy change, J/m^2.

The Gibbs free energy for the transformation from γ-Al_2O_3 to α-Al_2O_3 at different temperatures is calculated and plotted as a function of specific surface area in Fig. 5(a). The analysis reveals a critical specific surface area due to the differences in surface energy between γ-Al_2O_3 and α-Al_2O_3. When the specific surface area exceeds this critical value, γ-Al_2O_3 can be thermodynamically stabilized at elevated temperatures. At 1200, 1300, 1400, and 1500 ℃, the critical specific surface areas are 50.6, 44.9, 39.2, and 33.2 m^2/g, respectively.

The precursor was calcined at 1200 ℃ (a temperature at

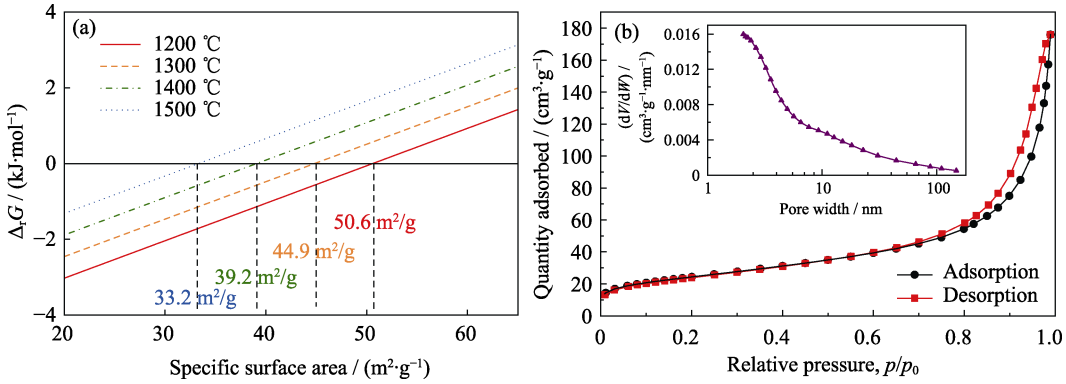

Fig. 5 (a) Gibbs free energy of the transformation from γ-Al_2O_3 to α-Al_2O_3 at different temperatures calculated as a function of specific surface area, and (b) N_2 adsorption-desorption isotherm of γ-Al_2O_3 with inset showing pore size distribution determined by application of BJH method to the isotherm

which the CRN reaction does not occur) for 4 h, followed by carbon removal at 700 ℃. The morphology of the resulting γ-Al_2O_3 is depicted in Fig. S10, revealing that it retains its plate-like shape and particle size consistent with that of the precursor. The specific surface area of γ-Al_2O_3 was measured by Brunauer-Emmett-Teller (BET) method. Fig. 5(b) presents the typical N_2 adsorption-desorption isotherm of γ-Al_2O_3. Barrett-Joyner-Halenda (BJH) method was employed to analyze the pore size distribution of γ-Al_2O_3, which ranged from 2 to 150 nm, exhibiting decreased pore volume with pore size increasing. The specific surface area of the obtained γ-Al_2O_3 is measured to be 87.5 m^2/g, which greatly exceeds the critical value.

Therefore, it can be reasonably inferred that the hydrothermal precursor, characterized by a unique core-shell structure with coated carbon that effectively inhibits the growth and agglomeration of alumina grains, maintains a high specific surface area during calcination. This guarantees the thermodynamical stability of γ-Al_2O_3 throughout the CRN process. As illustrated in Fig. S11, the atomic spacing in γ-Al_2O_3 crystals is larger than that in α-Al_2O_3 crystals, facilitating the diffusion of N atoms and O atoms at high temperatures, thereby promoting the CRN reaction. Tsuge *et al*.[39] investigated the reactivity of different crystalline forms of alumina (α-Al_2O_3, γ-Al_2O_3, η-Al_2O_3, θ-Al_2O_3, and $Al(OH)_3$) in the CRN reaction and found that γ-Al_2O_3 exhibited the highest reactivity. Therefore, it can be concluded that the combination of high specific surface area and thermodynamic stability of γ-Al_2O_3 significantly contributes to the superior reactivity of hydrothermal precursor in the CRN reaction.

3 Conclusions

AlN nanopowders were successfully synthesized through a combination of hydrothermal synthesis and CRN. A systematic investigation was conducted on the composition, structure, morphology, and generation mechanism of the products, leading to the following conclusions.

1) During the hydrothermal process, hydrothermal carbon and boehmite with opposite surface charges co-precipitate through electrostatic attraction to form precursors. The precursor exhibits a core-shell structure consisting of carbon-coated boehmite (γ-AlOOH@C), allowing for complete nanoscale contact between carbon and boehmite.

2) The highly reactive γ-Al_2O_3 nanoparticles and the extensive contact between alumina and carbon facilitate the hydrothermal precursor's participation in the CRN reaction, benefiting from thermodynamic and kinetic advantages. The CRN reaction initiates at 1300 ℃, with complete nitridation achieved at 1400 ℃ without the formation of α-Al_2O_3.

3) Taking the surface energy into account, the critical specific surface area is determined by thermodynamic calculations. The high-temperature stability of γ-Al_2O_3 during carbothermal reduction is quantitatively explained by the mitigation of surface area loss of γ-Al_2O_3 (87.5 m^2/g at 1200 ℃) due to carbon coating.

The findings from this work will also enhance the experimental and theoretical foundations for the preparation of other nitrides and carbides by a combination of hydrothermal synthesis and carbothermal reduction. Related research efforts are currently underway.

Supporting Materials

Supporting materials related to this article can be found at https://doi.org/10.15541/jim20240279.

References:

[1] YIM W M, PAFF R J. Thermal expansion of AlN, sapphire, and silicon. *Journal of Applied Physics*, 1974, **45(3):** 1456.

[2] SLACK G A, TANZILLI R A, POHL R O, *et al*. The intrinsic thermal conductivity of AIN. *Journal of Physics and Chemistry of Solids*, 1987, **48(7):** 641.

[3] SELVADURAY G, SHEET L. Aluminium nitride: review of synthesis methods. *Materials Science & Technology*, 1993, **9(6):** 463.

[4] RUTKOWSKI P J, KATA D. Thermal properties of AlN polycrystals obtained by pulse plasma sintering method. *Journal of Advanced Ceramics*, 2013, **2(2):** 180.

[5] SHEPPARD L M. Aluminum nitride: a versatile but challenging material. *American Ceramic Society Bulletin*, 1990, **69(11):** 1801.

[6] BAIK Y, DREW R A L. Aluminum nitride: processing and applications. *Key Engineering Materials*, 1996, **122:** 553.

[7] LEE H M, BHARATHI K, KIM D K. Processing and characterization of aluminum nitride ceramics for high thermal conductivity. *Advanced Engineering Materials*, 2014, **16(6):** 655.

[8] CHIKAMI H, FUKUSHIMA J, HAYASHI Y, *et al*. Kinetics of microwave synthesis of AlN by carbothermal-reduction-nitridation at low temperature. *Journal of the American Ceramic Society*, 2018, **101(11):** 4905.

[9] WANG Y M, QIAO L, ZHENG J W, *et al*. Preparation of AlN with low agglomeration using polyethylene glycol and emulsifier to disperse the ultrafine raw powders. *Ceramics International*, 2023, **49(1):** 1390.

[10] KOMEYA K, MATSUKAZE N, MEGURO T. Synthesis of AlN by direct nitridation of Al alloys. *Journal of the Ceramic Society of Japan*, 1993, **101(1180):** 1319.

[11] KIMURA I, ICHIYA K, ISHII M, *et al*. Synthesis of fine AlN powder by a floating nitridation technique using an N_2/NH_3 gas mixture. *Journal of Materials Science Letters*, 1989, **8(3):** 303.

[12] WEI Z L, LI K, GE B Z, *et al*. Synthesis of nearly spherical AlN particles by an *in-situ* nitriding combustion route. *Journal of Advanced Ceramics*, 2021, **10(2):** 291.

[13] YAMAKAWA T, TATAMI J, WAKIHARA T, *et al*. Synthesis of AlN nanopowder from γ-Al_2O_3 by reduction-nitridation in a mixture of NH_3-C_3H_8. *Journal of the American Ceramic Society*, 2006, **89(1):** 171.

[14] ZHANG Q H, GAO L. Synthesis of nanocrystalline aluminum nitride by nitridation of δ-Al_2O_3 nanoparticles in flowing ammonia.

Journal of the American Ceramic Society, 2006, **89(2):** 415.
[15] KIM J K, JUNG W S. Nitridation of *δ*-alumina to aluminum nitride under a flow of ammonia and its mechanism. *Journal of the Ceramic Society of Japan*, 2011, **119(1389):** 351.
[16] JUNG W S. Synthesis of aluminum nitride powder from *δ*-alumina nanopowders under a mixed gas flow of nitrogen and hydrogen. *Ceramics International*, 2012, **38(1):** 871.
[17] YOSHIMURA M, BYRAPPA K. Hydrothermal processing of materials: past, present and future. *Journal of Materials Science*, 2008, **43(7):** 2085.
[18] WANG Q, LI H, CHEN L Q, *et al*. Monodispersed hard carbon spherules with uniform nanopores. *Carbon*, 2001, **39(14):** 2211.
[19] GONG Y T, XIE L, LI H R, *et al*. Sustainable and scalable production of monodisperse and highly uniform colloidal carbonaceous spheres using sodium polyacrylate as the dispersant. *Chemical Communications*, 2014, **50(84):**12633.
[20] CHEN W, LI D, TIAN L, *et al*. Synthesis of graphene quantum dots from natural polymer starch for cell imaging. *Green Chemistry*, 2018, **20(19):** 4438.
[21] XIANG M, ZHOU Y, XU W, *et al*. Hydrothermal-carbothermal synthesis of highly sinterable AlN nanopowders. *Journal of the American Ceramic Society*, 2017, **100(6):** 2482.
[22] XIANG M, ZHOU Y F, XU W T, *et al*. Transparent AlN ceramics sintered from nanopowders produced by the wet chemical method. *Journal of the Ceramic Society of Japan*, 2018, **126(4):** 241.
[23] YANG J, CONG Y, LING J R, *et al*. Preparation of transparent AlON from powders synthesized by novel CRN method. *Journal of the European Ceramic Society*, 2022, **42(3):** 935.
[24] FANKHÄNEL J, SILBERNAGL D, GHASEM Z K M, *et al*. Mechanical properties of boehmite evaluated by atomic force microscopy experiments and molecular dynamic finite element simulations. *Journal of Nanomaterials*, 2016, **2016(1):** 5017213.
[25] WU J, XU W, DONG T, *et al*. Self-assembly of graphene reinforced ZrO_2 composites with deformation-sensing performance. *Ceramics International*, 2022, **48(21):** 32131.
[26] ANSI V A, SREELAKSHMI P, RAVEENDRAN P, *et al*. Table sugar derived carbon dot—a promising green reducing agent. *Materials Research Bulletin*, 2021, **139:** 111284.
[27] YANG J, WANG L H, JIANG X X, *et al*. AlN nanoparticles prepared through a gelation-polymerization process. *Ceramics International*, 2020, **46(11):** 17486.
[28] HE Q, QIN M L, HUANG M, *et al*. Mechanism and kinetics of combustion-carbothermal synthesis of AlN nanopowders. *Ceramics International*, 2017, **43(12):** 8755.
[29] MAO X X, XU Y G, MAO X J, *et al*. Synthesis of fine AlN powders by foamed precursor-assisted carbothermal reduction-nitridation method. *Journal of Inorganic Materials*, 2019, **34(10):** 1123.
[30] CARSTENS S, MEYER R, ENKE D. Towards macroporous α-Al_2O_3—routes, possibilities and limitations. *Materials*, 2020, **13(7):** 1787.
[31] CESTEROS Y, SALAGRE P, MEDINA F, *et al*. Several factors affecting faster rates of gibbsite formation. *Chemistry of Materials*, 1999, **11(1):** 123.
[32] MCHALE J M, NAVROTSKY A, PERROTTA A J. Effects of increased surface area and chemisorbed H_2O on the relative stability of nanocrystalline γ-Al_2O_3 and α-Al_2O_3. *The Journal of Physical Chemistry B*, 1997, **101(4):** 603.
[33] MCHALE J M, AUROUX A, PERROTTA A J, *et al*. Surface energies and thermodynamic phase stability in nanocrystalline aluminas. *Science*, 1997, **277(5327):** 788.
[34] BLONSKI S, GAROFALINI S H. Molecular dynamics simulations of α-alumina and γ-alumina surfaces. *Surface Science*, 1993, **295(1/2):** 263.
[35] TASKER P W. Surfaces of magnesia and alumina. *Advances in Ceramics*, 1984, **10:** 176.
[36] MACKRODT W C, DAVEY R J, BLACK S N, *et al*. The morphology of α-Al_2O_3 and α-Fe_2O_3: the importance of surface relaxation. *Journal of Crystal Growth*, 1987, **80(2):** 441.
[37] CAUSÀ M, DOVESI R, PISANI C, *et al*. *Ab initio* characterization of the (0001) and (10$\bar{1}$0) crystal faces of α-alumina. *Surface Science*, 1989, **215(1/2):** 259.
[38] CASTRO R H R, USHAKOV S V, GENGEMBRE L, *et al*. Surface energy and thermodynamic stability of γ-alumina: effect of dopants and water. *Chemistry of Materials*, 2006, **18(7):** 1867.
[39] TSUGE A, INOUE H, KASORI M, *et al*. Raw material effect on AlN powder synthesis from Al_2O_3 carbothermal reduction. *Journal of Materials Science*, 1990, **25(5):** 2359.

水热-碳热合成 AlN 纳米粉体的机理

冯关正[1,2,3], 杨 健[1,2], 周 渡[1,2], 陈啟明[1,2,3], 许文涛[1,2], 周有福[1,2]

(1. 中国科学院 福建物质结构研究所, 光电材料化学与物理重点实验室, 福州 350002; 2. 福建光电信息科技创新实验室, 福州 350108; 3. 中国科学院大学, 北京 100039)

摘 要: 碳热还原氮化法是应用最广泛的制备 AlN 粉体的方法。该工艺制备的 AlN 粉体纯度高且烧结活性优良, 但是存在反应温度高、原料难以混合均匀等不足。本研究将水热合成与碳热还原氮化法相结合制备 AlN 纳米粉体。以硝酸铝为铝源、蔗糖为碳源、尿素为沉淀剂, 在 200 ℃水热合成碳和勃姆石(γ-AlOOH)均质复合前驱体。前驱体通过静电吸引形成碳紧密包覆勃姆石的核壳结构(γ-AlOOH@C)。与传统前驱体相比, 水热复合物具有超细颗粒、粒度分布均匀、分散性好、反应活性高、环境友好等优点。在氧化铝相的稳定性方面, 碳壳通过抑制氧化铝的表面积损失, 使 γ-Al_2O_3 相比刚玉相(α-Al_2O_3 相)的热稳定性更好, γ-Al_2O_3 在碳热还原过程中能保持较高的反应活性, 该反应始于 1300 ℃, 止于 1400 ℃(比传统碳热还原法低 200 ℃)。本研究通过实验和热力学计算验证了相关机理, 为水热法结合碳热法制备非氧化物纳米陶瓷粉体提供了有效的理论和实验依据。

关 键 词: 氮化铝; 碳热还原氮化法; 机理; 水热合成; 前驱体

中图分类号: TM282 **文献标志码:** A **文章编号:** 1000-324X(2025)01-0104-07

Supporting Materials:

Mechanism for Hydrothermal-carbothermal Synthesis of AlN Nanopowders

FENG Guanzheng[1,2,3], YANG Jian[1,2], ZHOU Du[1,2], CHEN Qiming[1,2,3], XU Wentao[1,2], ZHOU Youfu[1,2]

(1. Key Laboratory of Optoelectronic Materials Chemistry and Physics, Fujian Institute of Research on the Structure of Matter, Chinese Academy of Sciences, Fuzhou 350002, China; 2. Fujian Science & Technology Innovation Laboratory for Optoelectronic Information of China, Fuzhou 350108, China; 3. University of Chinese Academy of Sciences, Beijing 100039, China)

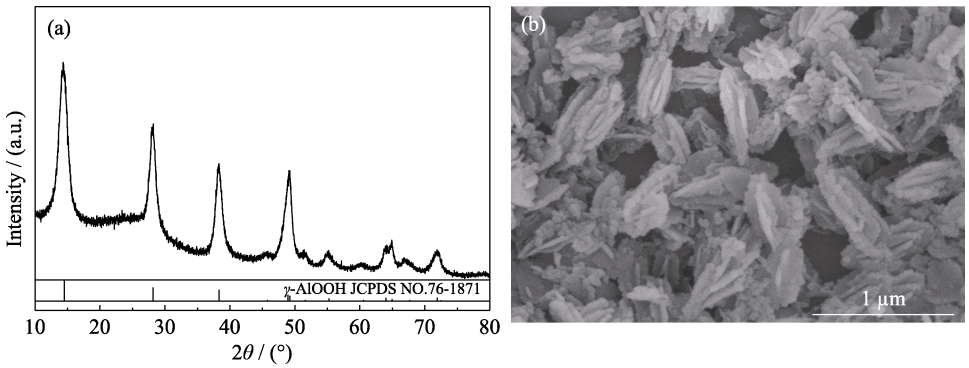

Fig. S1　(a) XRD pattern and (b) FESEM image of the precursor obtained at 200 ℃

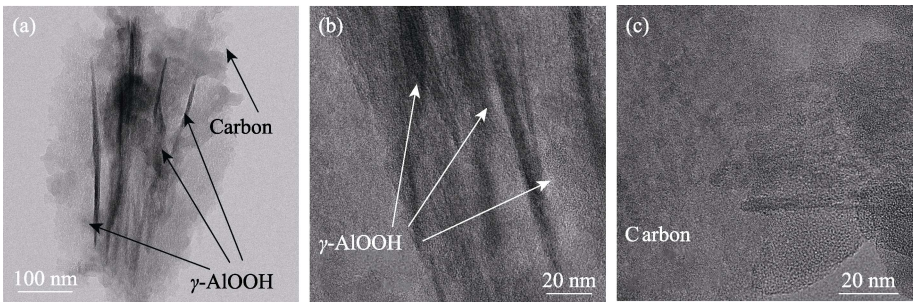

Fig. S2　TEM images of the precursor

(a) Precursor; (b) γ-AlOOH; (c) Carbon

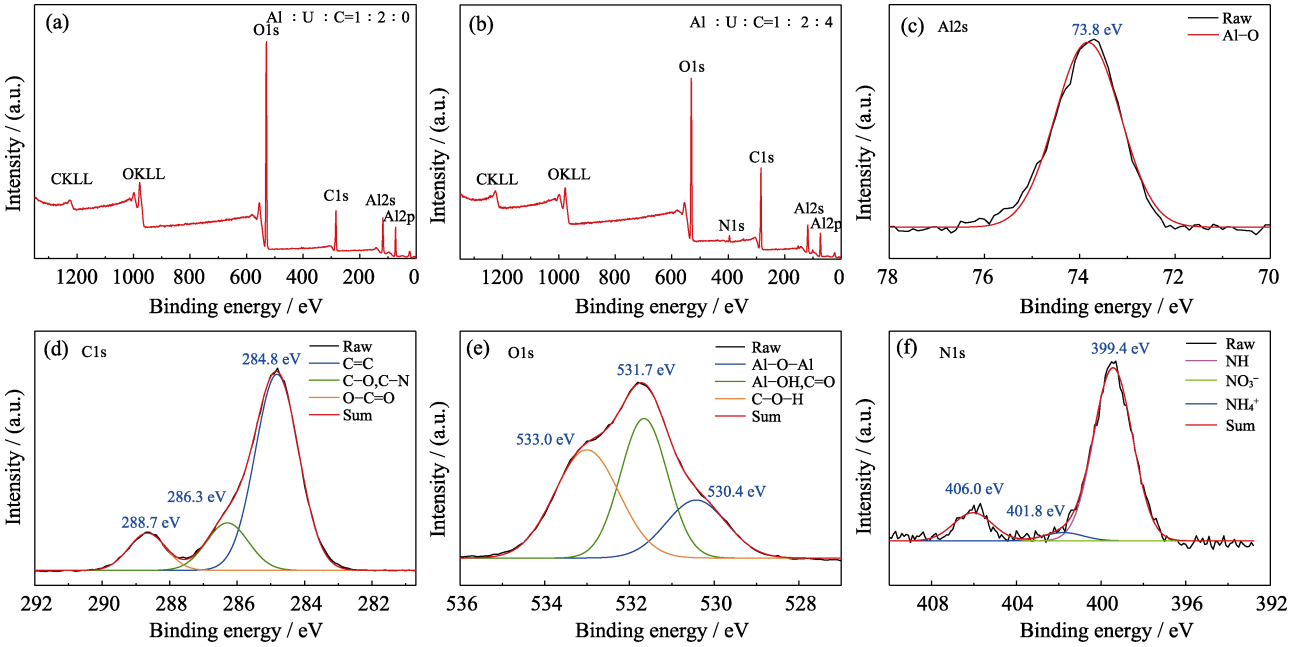

Fig. S3　(a, b) Survey spectra of the precursors at (a) Al : U : C=1 : 2 : 0 and (b) Al : U : C=1 : 2 : 4; (c-f) XPS spectra of (c) Al2s, (d) C1s, (e) O1s, and (f) N1s for the precursors at Al : U : C=1 : 2 : 4

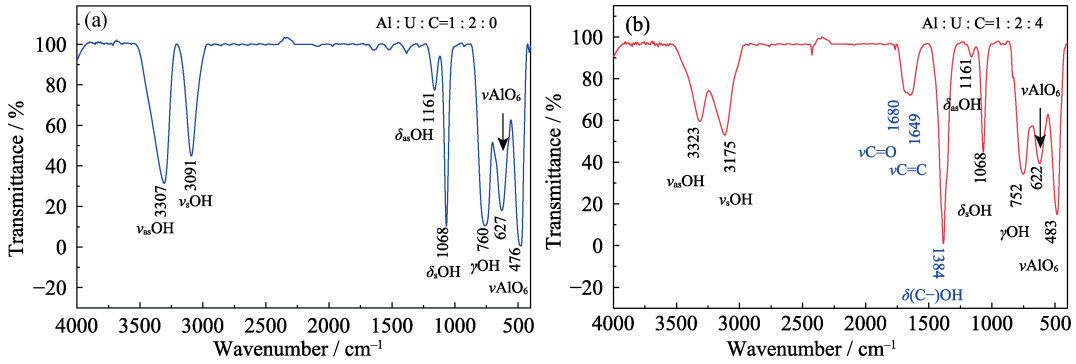

Fig. S4 FTIR spectra of the precursors

(a) Al : U : C=1: 2: 0; (b) Al : U : C=1 : 2 : 4

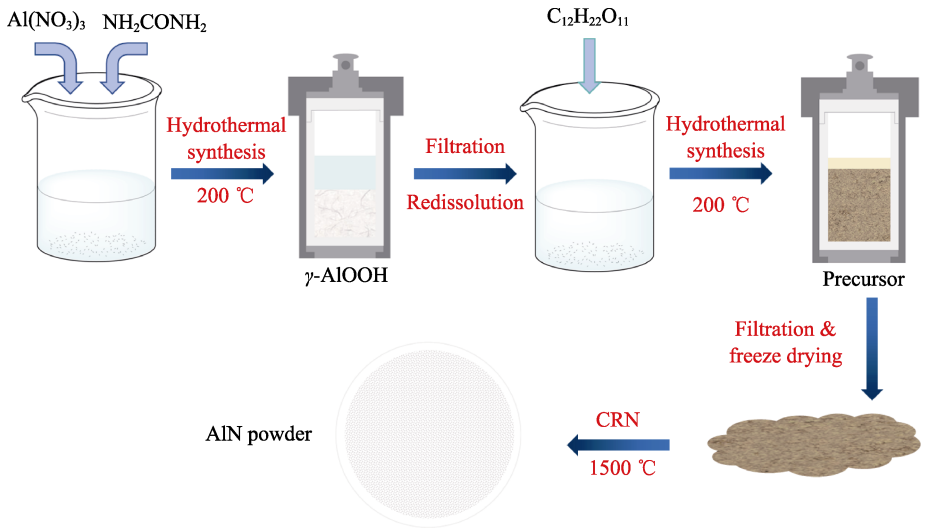

Fig. S5 Experimental procedure for validating the mechanism of precursor formation through electrostatic adsorption

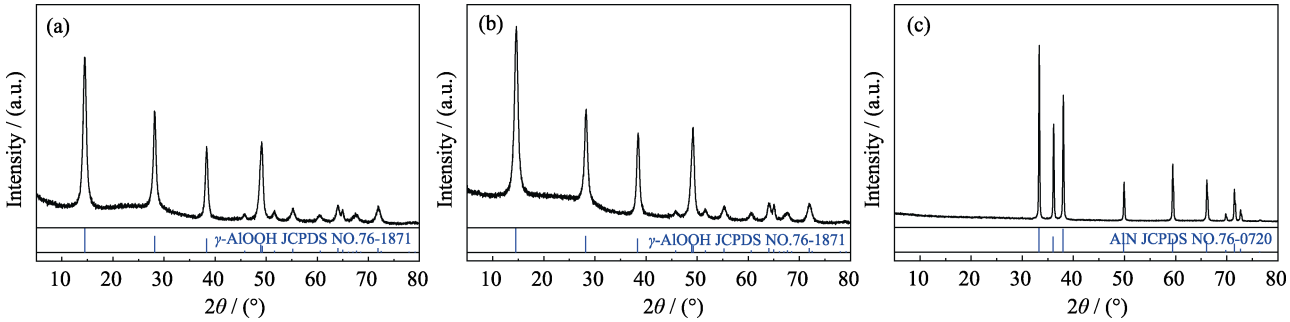

Fig. S6 XRD patterns of the products in Fig. S5

(a) Boehmite; (b) Precursor; (c) AlN

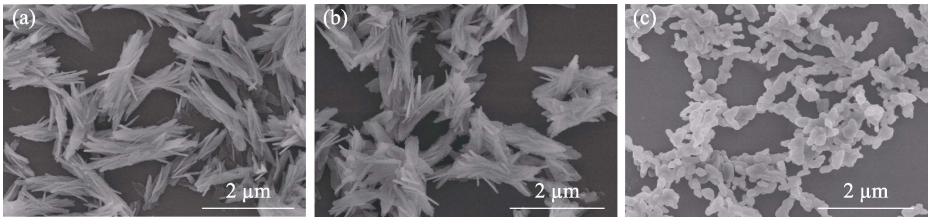

Fig. S7 FESEM images of the products in Fig. S5

(a) Boehmite; (b) Precursor; (c) AlN

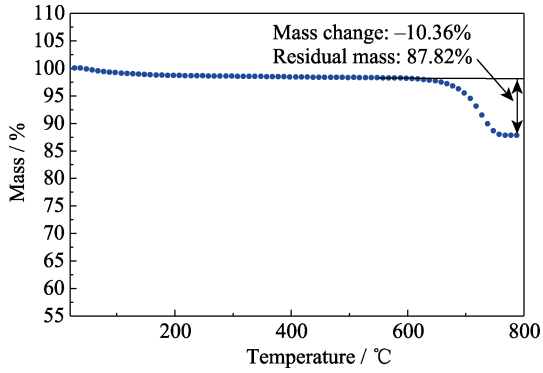

Fig. S8　TGA curve of the product calcined at 1400 ℃ in air

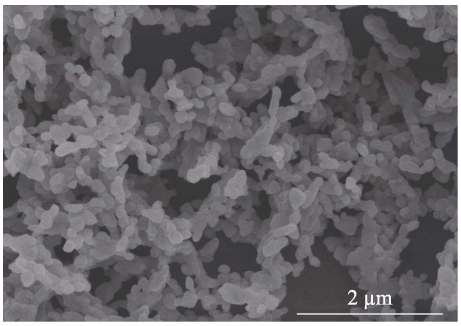

Fig. S9　FESEM image of AlN nanopowder produced at 1400 ℃

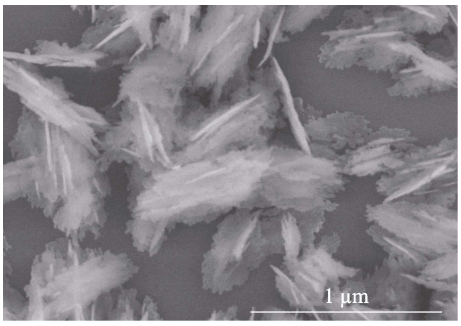

Fig. S10　FESEM image of the product after calcination at 1200 ℃ and carbon removal at 700 ℃

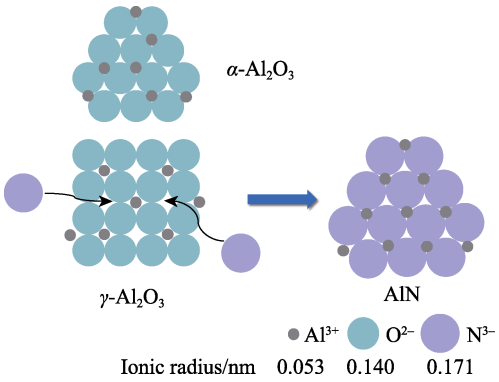

Fig. S11　Structure diagram of α-Al_2O_3, γ-Al_2O_3 and AlN